Fabrication of burst pressure competent vascular grafts via electrospinning: Effects of microstructure

Sarah Drilling, Jeremy Gaumer, John Lannutti
Department of Materials Science and Engineering, The Ohio State University, 2041 College Rd., Columbus, Ohio 43210

Received 6 July 2007; revised 11 September 2007; accepted 27 November 2007
Published online 2 April 2008 in Wiley InterScience (www.interscience.wiley.com). DOI: 10.1002/jbm.a.31926

Abstract: In this work, electrospun tubes of interest for vascular tissue engineering were fabricated and evaluated for burst pressure and suture retention strength (SRS) in the same context as tensile strength providing a direct, novel comparison. Tubes could be fabricated displaying average burst pressures up to 4000 mmHg—well above the standard of 2000 mmHg—and SRS values matching those of relevant natural tissues. Surprisingly, highly oriented fiber and maximal tensile properties are not absolutely necessary to attain clinically adequate burst pressures. The ability to resist bursting is clearly related to both initial solution solids loading and electrospinning deposition time. We make novel *in situ* observations of the relative microstructural characteristics of failure during bursting, and connect this to the conditions used to fabricate the graft. Processes typically thought to promote fiber alignment are, in fact, highly condition-dependent and do not always provide superior properties. In fact, electrospun structures displaying no discernable alignment could achieve burst pressures regarded clinically sufficient. The properties of individual electrospun fiber clearly do not fully dictate macroscale properties. Normal background levels of point bonding are enhanced by increased rotational speeds, and can have effects on properties more dominant than those of alignment. © 2008 Wiley Periodicals, Inc. J Biomed Mater Res 88A: 923–934, 2009

Key words: biodegradable; electrospinning; bioengineering; burst pressure; biomaterials

INTRODUCTION

Coronary vascular disease is the leading cause of morbidity and mortality in the US; over 2 million surgical or percutaneous procedures are performed annually.[1] Although vascular bypass grafting remains the mainstay revascularization treatment for ischemic heart disease and peripheral vascular disease, many patients do not have healthy vessels suitable for harvest. In addition, the patient population undergoing repeat coronary revascularization is increasing; ~15% of these patients will require alternative conduits.[2] Pre-existing conditions may limit the availability of suitable autogenous vessels for complete coronary revascularization. Thus, there is an increased need for alternative, synthetic, small-diameter vascular grafts. Unfortunately, the use of synthetic materials is limited to grafts larger than 5–6 mm, because of the frequency of occlusion observed with small-diameter prosthetics.[3,4]

In 1952, Voorhees and Ah likely developed the first synthetic fiber-based vascular graft when they constructed vascular prostheses out of Vinyon N.[5] Since that time, many researchers have pursued production of the "ideal" synthetic vascular graft. Although many materials have been considered as grafts, Dacron (polyethylene terephthalate) and expanded polytetrafluoroethylene (ePTFE) grafts have emerged as the primary synthetics in clinical use.[6] Although large diameter grafts provide long-term patency rates,[7] smaller diameter (<5 mm) grafts suffer early thrombotic complications and late myointimal hyperplasias, often leading to total graft occlusion.[3] In fact, less than 50% of small diameter femoropopliteal grafts remain patent 5 years postimplantation.[4]

In the face of these limitations, investigators have turned their attention toward seeding vascular grafts with endothelial cells to improve long-term patency. Such tissue engineering approaches

Correspondence to: J. Lannutti; e-mail: lannutti.1@osu.edu
Contract grant sponsor: National Science Foundation; contract grant number: EEC-0425626

are actively being pursued to add the only truly nonthrombogenic surface—the human endothelium—to the luminal wall of otherwise synthetic grafts. By exploiting the ability of endothelial cells to inhibit the full range of blood response to any synthetic surface, investigators hope to develop the first true cellular therapy treating cardiovascular disease. Herring and Glover made the first report of such a seeded graft in 1978.[8] In subsequent studies, it was realized that while cell source and seeding technique are important to ultimate seeding efficiency, the substrate/scaffold upon which the cells are seeded is a primary determinant of optimal graft endothelialization and subsequent success *in vivo*.

A well-designed vascular scaffold must also meet two specific mechanical requirements to be effective: (1) it must retain microstructural integrity and stability after implantation and (2) it must provide sufficient biomechanical support. In producing substrates for vascular engineering, adequate burst pressure is a critical goal.[9–20] The imposed requirement of 2000 mmHg is mandated by both clinical concerns[18] and the fact that the arteries targeted for replacement typically have burst pressures above 2000 mmHg.[13]

In pursuit of such mechanically capable scaffolds we utilized electrospinning, fast becoming a standard method of preparing tissue engineering scaffolds. We chose polycaprolactone (PCL) as a biodegradable alternative to Dacron or PTFE. PCL has a good short-term load bearing ability due to its relatively slow degradation rate *in vivo*.[21] Electrospun PCL has previously been used as a scaffolding for bone[22–25] and cartilage[26–28] to support cell proliferation and extracellular matrix (ECM) deposition, and we have considerable experience with both this and electrospinning.[29–33]

To our knowledge, no previous studies of electrospun PCL have achieved the 2000 mmHg burst pressures required for clinical application as vascular grafts. Studies have shown that electrospun nanofibrous structures have better mechanical properties than do structures composed of larger diameter fibers.[34] Fortunately, this process can easily be used to fabricate tubular constructs[35–40] suitable for subsequent cell seeding.[41] Unfortunately, these constructs do not always exhibit appropriate biomechanical properties. The concept of fiber alignment[42–47] is often put forward as a means of improving mechanical behavior. Little is known, however, about the microstructural characteristics of these "aligned" structures and how these may control burst pressure and suture retention. Here, we report our procedures for generating electrospun grafts having appropriate burst pressures and their microstructural behavior under loading regimes considered clinically relevant.

MATERIALS AND METHODS

Electrospun PCL

Solutions (12, 18, and 25 wt %) of poly(ϵ-caprolactone) (PCL, Sigma-Aldrich, M_w = 65,000) in acetone (Mallinckrodt Chemicals) and 6.7 wt % PCL in hexafluoroproponal (HFIP, Mallinckrodt Chemicals) were prepared by heating the solvents to 50°C, while continuously stirring to fully dissolve introduced PCL. The use of 6.7 wt % PCL in HFIP follows after the work of Zhang et al.[48], who used 10 w/v % PCL in TFE; conversion to wt % in HFIP results in the 6.7% value. After cooling to room temperature, the solutions were deposited onto a target using a 20-gauge blunt tip needle under a 24-kV potential. A 15-cm tip-to-mandrel distance and a 20 mL/h flow rate were employed. For sheet tensile specimens, the collector plate was a 6.35 cm × 6.35 cm square covered with aluminum foil. For the tangential and longitudinal tensile specimens, a grounded 1.27-cm diameter mandrel was spun at 2500 rpm (a linear tangential velocity of 0.65 m/s) and used to collect fibers. These two speeds, 0.65 and 1.66 m/s, are both much lower than the >4 m/s needed to observe statistical differences in ultimate tensile strength (UTS).[49] For burst pressure and suture retention strength (SRS) samples, a grounded 5-mm diameter mandrel was spun at 2500 rpm (a linear tangential velocity of 1.66 m/s), while collecting fibers. The total deposition time for the tensile specimens was 10 min. For burst pressure samples, it ranged from 5 to 10 min, unless otherwise indicated. For SRS samples, deposition required 5 min. Both the tubes used to evaluate burst pressure and the tubes used to produce tensile specimens were generated from 7.6-cm long tubes. Uniformity of tube wall thicknesses along the length of the mandrel was evaluated by spinning samples (n = 5) of each composition for 7 min and recording their diameter with a laser micrometer (TLA, LS-7030). The scans consisted of >700 diametric measurement along an 8-cm length of the tubes, providing the following averages and standard deviations: 618 ± 58 μm (12 wt % in acetone), 900 ± 60 μm (18 wt % in acetone), 1057 ± 172 μm (25 wt % in acetone), 331 ± 90 μm (6.7 w/v % in HFIP). The SRS tubes were 3-cm long. All samples were placed in a vacuum overnight to ensure that the residual solvent levels in the electrospun polymer were below toxic levels.[29]

The 12, 18, and 25 wt % PCL spun from acetone are hereafter referred to as 12, 18, and 25 wt % PCL. The 6.7 wt % PCL spun from HFIP is hereafter referred to as 6.7 wt % HFIP PCL.

Tensile strength

Tensile dog bones with a gauge length of 20 mm and a width of 2.4 mm were cut by placing the sheet between two 2-mm thick aluminum templates. A Bard-Parker No. 15 surgical blade was used to cut the straight edges, while a 3-mm dermal punch was used to cut the radii. Great care was taken to ensure that no tearing or smearing of the electrospun PCL occurred. Tensile sample thickness was measured using a digital micrometer: the gauge length of each specimen was confined between two glass microscope slides and the total thickness determined. Subtraction of the thicknesses of the individual glass slides provided an average gauge length thickness. The tensile properties were determined utilizing a 1-kg load cell (model 31, Sensotec) and a strain rate of 5 mm/min on an Instron load frame (model 1322) using lightweight carbon fiber grips (A2-166 Fiber Clamp Assembly, Instron). The sample size (n) per condition was five. To calculate the modulus from the sheet, tangential, and longitudinal tensile specimens, stress and strain values between 0 and 10% strain (∼30 data points) were used.

Burst pressure

Using the appropriate electrospun tubes, an angioplasty balloon having the matching diameter was first evacuated and then inserted into the graft. The balloon was then filled with water at a rate of 20 mL/min and the graft allowed to lengthen freely until bursting occurred.[50] The balloon + graft diameter was actively measured using a laser micrometer (Keyence LS-7001 high accuracy CCD); the inflation pressure was also recorded using a transducer (Honeywell 40PC150G) connected to a data acquisition board (National Instruments Co., Austin, TX) during filling. The data was recorded using a LabView.vi system. The burst pressure was defined as the highest pressure reached before failure up to the 5000 mmHg limit for this system. An $n = 5$ was used for each data point.

As-strained burst pressure microstructures

To examine the strained electrospun microstructure in the as-inflated condition, the angioplasty balloon was first inserted into each graft and inflated until the sample reached ∼40% diametric strain. The sample did not fail, but displayed visible regions of strain and deformation. A stopcock was then used to maintain the pressure inside the balloon and the combination placed into a plastic bag that was then inserted into a circulating water bath at 50°C for 10 min. This thermal exposure caused extensive "necking" to develop between the fibers[51] and prohibited free fiber motion, while also relaxing diametric strains incurred during testing. The samples were then placed on double-sided carbon tape, and gold coated and prepared for scanning electron microscopy (SEM) [see Section "Scanning electron microscopy (SEM)"].

Suture retention strength (SRS)

To measure the force necessary to pull a suture through the wall of an electrospun graft, two types of cuts were used: "straight across" and "oblique."[52] The straight across method uses a graft cut normal to the long axis producing sections ∼18 mm in length. Three silk sutures (6.0 Ethicon with a cutting needle) are inserted 2 mm from the end of the graft at 90° angles, looped, and tied with seven knots.[9] The suture loop and the other end of the graft are secured to the grips of the tensile machine using a 22.7-kg (50 lb) load cell (Test Resources, MTestW R system) and pulled at 50 mm/min, until the suture pulled through the vessel wall. The maximum force required is the SRS. The oblique method is similar, but the graft is cut at 45° to the long axis and single sutures are located at the base (heel) of the cut, the toe of the cut, and at 90° to the toe. The electrospun samples were oriented such that the sutures pulled out parallel to the longitudinal axis of the tube (perpendicular to any potential orientation).

Scanning electron microscopy (SEM)

Determination of microstructural change (or its absence) required that these samples be examined in an SEM (FEI Sirion) at accelerating voltages of 5–15 kV. All samples were coated with gold (Pelco Model 3 Sputter Coater 9100). Great care was taken to make sure that the fibers were not excessively heated during sputter coating. In all cases, measurements of fiber orientation and diameter were made utilizing 100–200 fibers, following the procedures given in the pioneering work of Inai et al.[53]

RESULTS

Tensile testing

Figure 1 shows that UTS is highly dependent upon the solids loading of the acetone, as each concentration produces a clearly characteristic value. The 12 wt % loading average is ∼37.9 and 58.4% of the average 18 and 25 wt % values, respectively. The choice of HFIP as a solvent produces the more "classic" behavior expected from electrospun fiber aligned by the action of a rotating mandrel. In comparison to 18 wt % acetone, 6.7 wt % PCL in HFIP in the tangential direction shows a dramatic 3- to 4-fold increase in UTS. The longitudinal direction displays a strength value even lower than either the 12

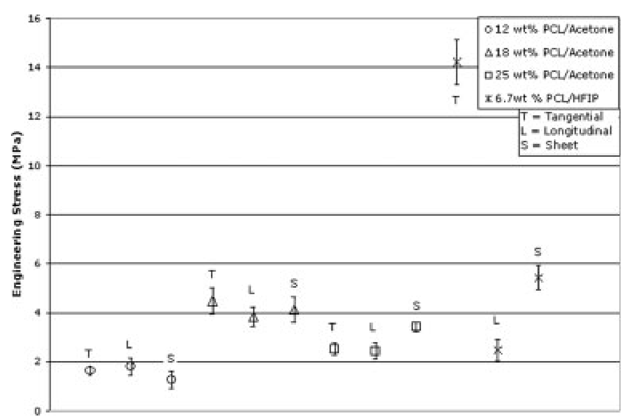

Figure 1. UTS of the PCL-solvent compositions. T = tangential (in the direction of the intended orientation); L = longitudinal (transverse to the intended orientation); S = sheet (unoriented).

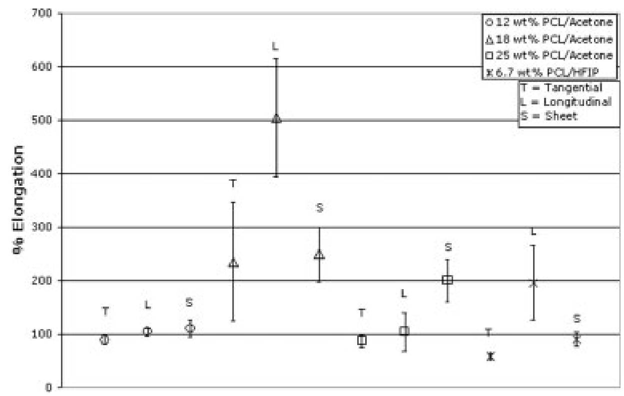

Figure 2. Strain data from the PCL-solvent compositions. T = tangential (in the direction of the intended orientation); L = longitudinal (transverse to the intended orientation); S = sheet (unoriented).

or the 18 wt % average, while the sheet condition is only 49% of the longitudinal value for 18 wt %.

In contrast, the strain data (Fig. 2) shows more dramatic variations. The 12 wt % data is remarkably uniform around 100% strain regardless of direction/condition. Relative to itself, the 18 wt % displays a substantial increase in the longitudinal versus the tangential direction (from 235 to 505%). Interestingly, the sheet condition displays a value very similar to that of the tangential direction. All three acetone conditions show relatively large standard deviations. The 25 wt % data, in turn, is similar to the 12 wt % data in both value and consistency although the sheet condition, surprisingly, provides for greater total strain. Concurrently, the strain data shows that the 6.7 wt % HFIP data produces a tight clustering at an average of 50% strain in the tangential direction, a wider range of strains (~130 to 270%) in the longitudinal direction, and 75–110% strain in the sheet condition. As expected for highly aligned materials, total elongation to failure decreases compared to the 18 wt % PCL composition.

Figure 3 shows that acetone compositions (12, 18, and 25 wt % PCL) result in clustering of the modulus values not present in the 6.7 wt % PCL HFIP data (see inset) that varies widely. The tangential 6.7 wt % PCL HFIP data has a modulus identical to the sheet data, but its UTS is more than twice as large. Not surprisingly, the longitudinal direction displays a lower average for 6.7 wt % PCL HFIP. The longitudinal data consistently show the lowest values for each spinning parameter. Sheet tensile specimens had the highest average value regardless of spinning parameter. Quantitative data reporting both modulus and average UTS is found in Table I.

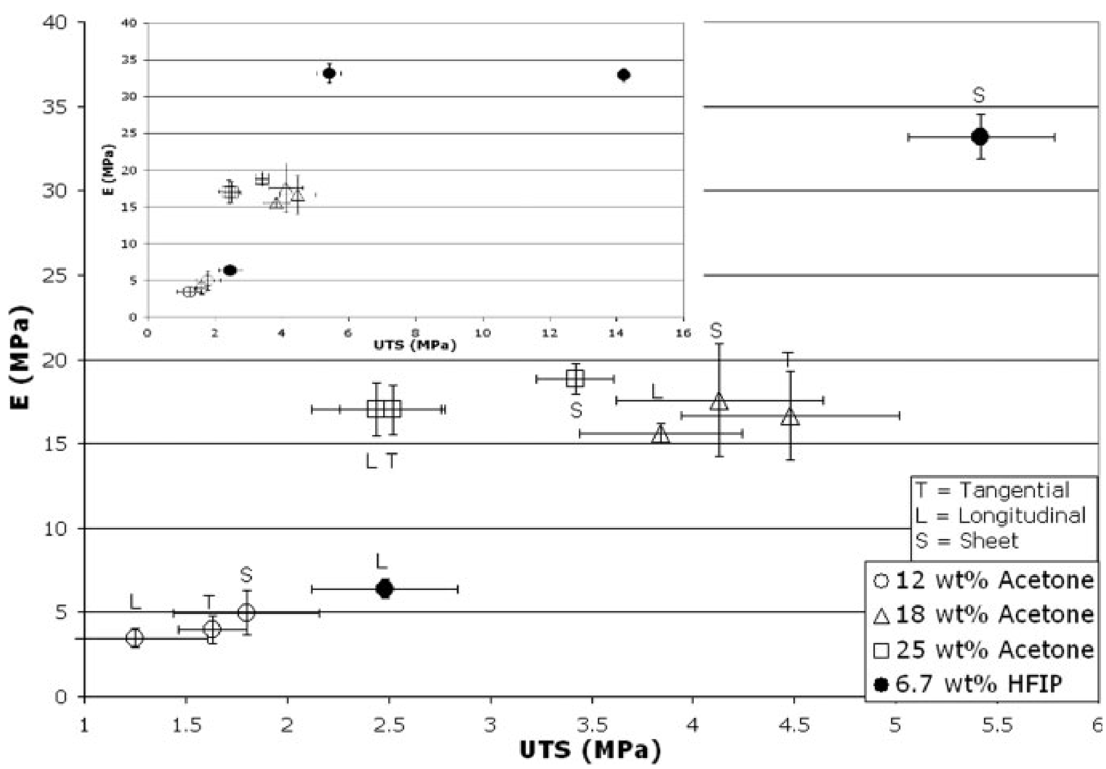

Figure 3. Modulus versus solvent identity and solids loading. Acetone compositions (12, 18, and 25 wt % PCL) result in clustering not present in 6.7 wt % PCL HFIP data (see inset) that varies widely. Not surprisingly, the longitudinal direction displays a lower average for 6.7 wt % PCL HFIP. The tangential 6.7 wt % PCL HFIP data is plotted in the upper right-hand corner of the inset) has a modulus identical to the sheet data but its UTS is more than twice as large.

TABLE I
Modulus and Average UTS of the Different Samples and Tensile Directions

Solution (wt % PCL/ Solvent)	Orientation	E (MPa)	UTS (MPa)
12/acetone	Tangential	3.95 ± 0.82	1.63 ± 0.17
	Longitudinal	3.49 ± 0.56	1.25 ± 0.36
	Sheet/random	4.96 ± 1.30	1.8 ± 0.36
18/acetone	Tangential	16.65 ± 2.62	4.48 ± 0.54
	Longitudinal	15.61 ± 0.63	3.84 ± 0.40
	Sheet/random	17.60 ± 3.35	4.13 ± 0.51
25/acetone	Tangential	17.00 ± 1.44	2.52 ± 0.26
	Longitudinal	17.07 ± 1.57	2.44 ± 0.32
	Sheet/random	18.81 ± 0.88	3.42 ± 0.19
6.7/HFIP	Tangential	32.94 ± 6.62	14.22 ± 0.90
	Longitudinal	6.38 ± 1.87	2.48 ± 0.44
	Sheet/random	33.18 ± 3.31	5.42 ± 0.50

Microstructure

Figure 4 shows that for 12 wt % PCL spun onto a mandrel [Fig. 4(a)], slight beading occurs and is not accompanied by measurable alignment [Fig. 5(a)]. Figure 5 shows that for 18 wt % PCL spun onto a mandrel [Fig. 4(b)], alignment is more obvious and can be measured [Fig. 5(b)]. In contrast to Figure 4(a), no obvious beading results from these spinning conditions. Upon close examination, point bonding between fibers can be observed but is, as usual, difficult to quantify. Figure 5 also shows that for 25 wt % PCL [Fig. 4(c)] spun onto a rotating mandrel, only limited (if any) alignment can be measured [Fig. 5(c)]. In contrast to Figure 4, obvious point bonding results from these spinning conditions. Figure 5 also shows that for 6.7 wt % PCL in HFIP [Fig. 4(d)] spun onto the rotating mandrel, clear evidence of alignment is observed [Fig. 5(d)]. Point bonding—resulting from the use of a too-short source-ground distance—apparently compromises the effects of orientation resulting from these spinning conditions. The average fiber diameters for 12, 18, and 25 wt % PCL in acetone are 610, 1370, and 2280 nm, respectively. The average diameter of the 6.7 w/v % PCL in HFIP fibers is 790 nm.

Burst pressure results

Figure 6 shows steady progress toward the standard goal of 2000 mmHg[13,18] resulting in spinning conditions that either meet or exceed this goal. In electrospun scaffolds, the ability to resist bursting is related to both solids loading and deposition time. However, burst pressure clearly does not follow the

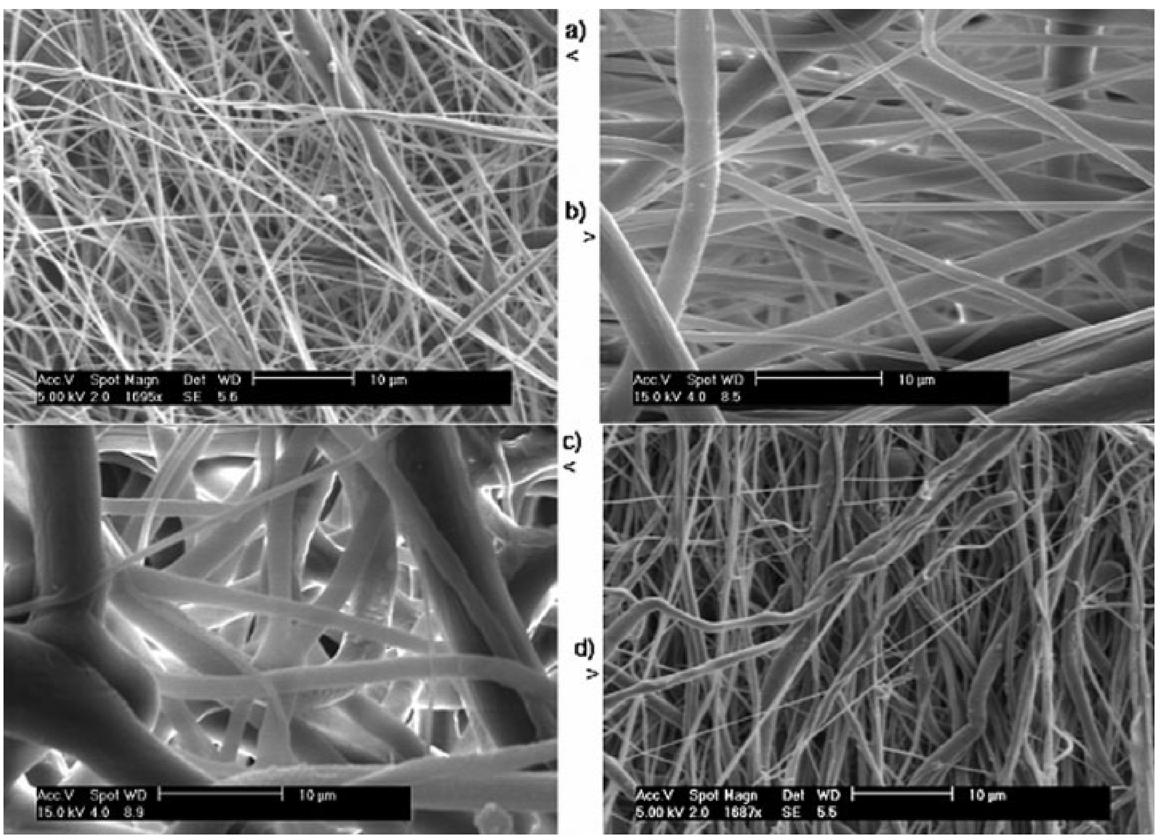

Figure 4. SEM images of mandrel-deposited electrospun PCL fibers. a) 12 wt %; b) 18 wt %; c) 25 wt %; d) 6.7 wt % HFIP PCL. The tangential direction is the vertical direction in all but b) where the tangential direction is horizontal.

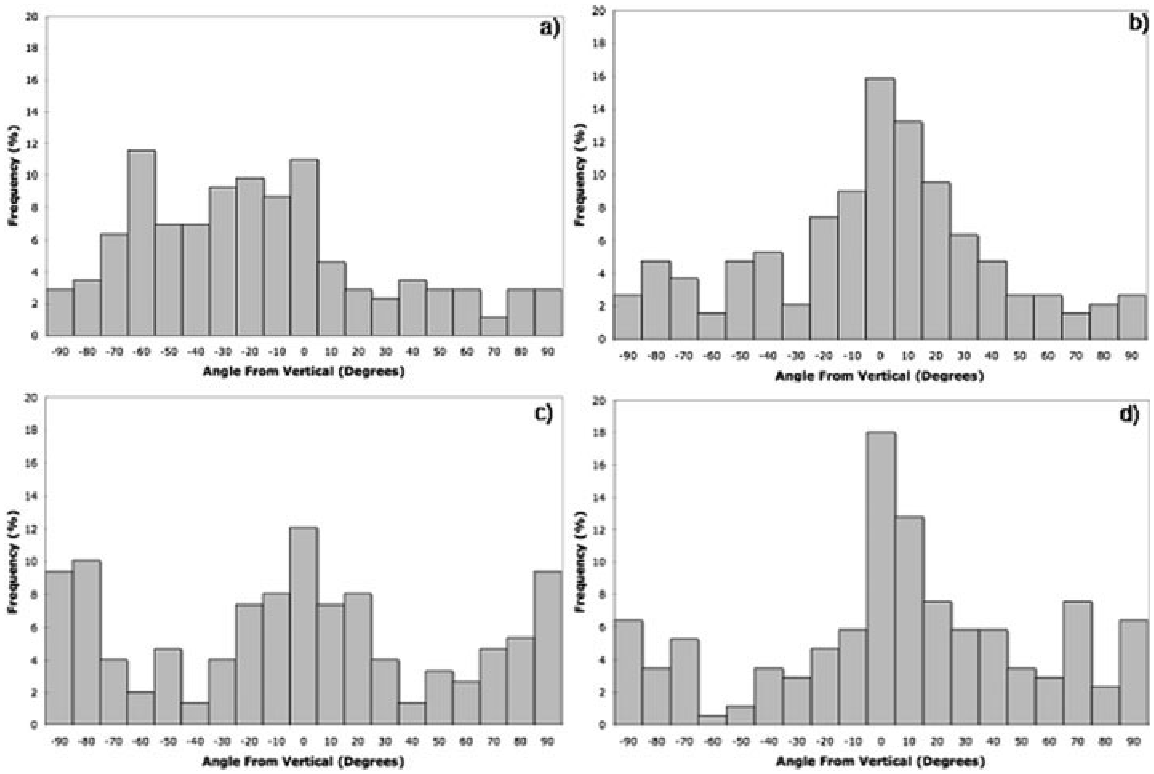

Figure 5. Orientational measurements taken from the images in Figure 6 of mandrel-deposited electrospun PCL fibers. a) 12 wt %; b) 18 wt %; c) 25 wt %; d) 6.7 wt % HFIP PCL.

trends observed during tensile testing, in that the 7-min 25 wt % (displaying a UTS of 2.5 MPa in the tensile direction) clearly resists bursting more effectively than the 7-min 18 wt % (4.5 MPa in the tensile direction). To date, HFIP displays the greatest resistance to bursting, and this is more consistent with the tensile results. Slight sintering[51] of the 12 and 18 wt % fibers to produce more point bonding between the individual fibers does not result in significant increases in burst pressure.

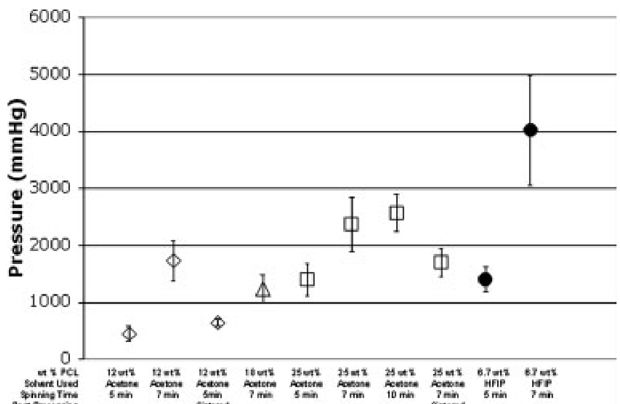

Figure 6. Burst pressure versus electrospinning conditions. Only the 25 wt % PCL and 6.7 wt % PCL HFIP cases achieved clinically desirable burst pressures.

Figure 7 shows a low magnification result of *in situ* microstructural analysis of the 18 wt % PCL tubular grafts subjected to diametric strain utilizing the burst pressure apparatus. This reveals a size-based hierarchical arrangement of fibers and defects in the strained microstructure. Figure 8(a) shows the typical *in situ* response the acetone-based composi-

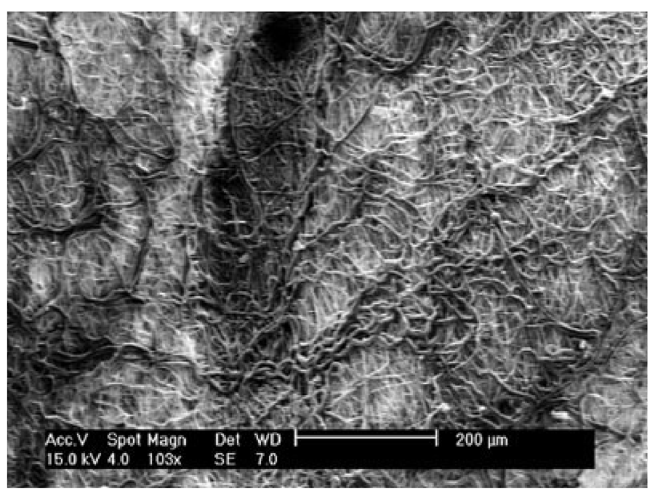

Figure 7. A low magnification view of the 18 wt % PCL structure under sustained 41.5% diametric strain. Note the distribution of large and small fiber diameters and the segregation of the larger fibers into braided structures.

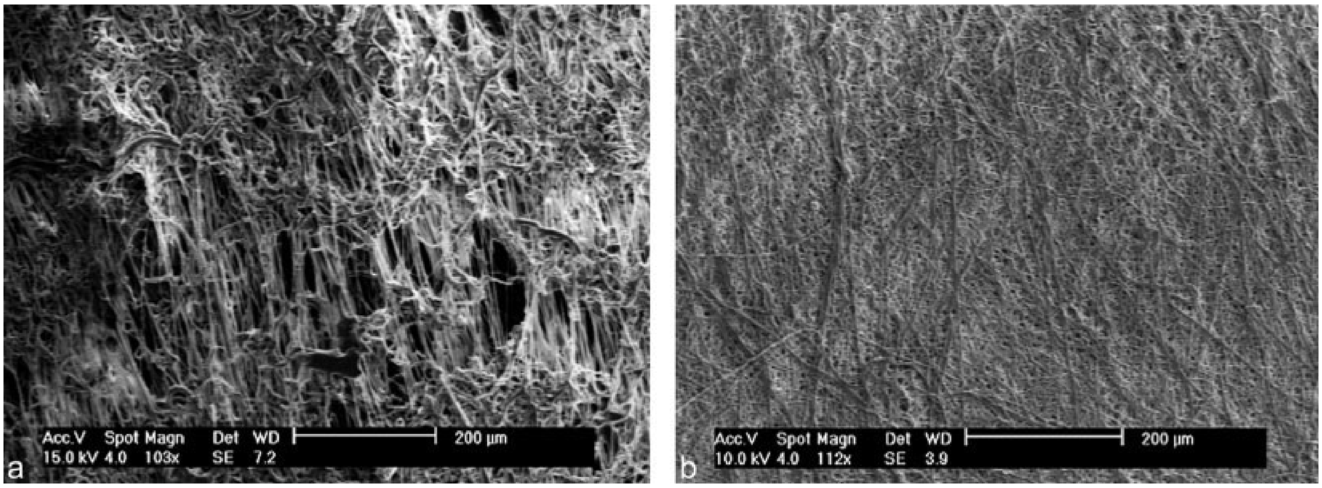

Figure 8. Low magnification views of (a) 25 wt % PCL at 45.7% diametric strain and (b) 6.7 wt % PCL HFIP at 42.8% diametric strain. The acetone-based compositions show the pictured localization of stress between braided fiber in between which aligned fibers are visible. In contrast, the HFIP-based composition shows only moderately aligned fiber free of the obvious areas of localized deformation in (a).

tions, in which strain is accommodated by the generation of a network structure where the edges of expanding defects are composed of larger diameter fiber apparently collected into continuous "braided" structures. This low magnification view reveals what appears to be a large (350–500 µm) defect growing within the microstructure. Within this defect, alignment of smaller diameter fibers is obvious. Given the broad distribution of fiber diameters that are generated during electrospinning, this could be due to higher levels of point bonding[51,54] that logically should exist due to relatively prolonged retention of solvent in these larger diameter fibers.

In the HFIP-generated fiber [Fig. 8(b)], in contrast, increases in pressure are accommodated by increased alignment rather than the generation of individual defects. Visual observations of failure show that HFIP-based fiber grafts undergo catastrophic failure with no obvious point of initiation. The acetone-based compositions always exhibit a momentary local failure (in which the internal balloon briefly extrudes through the wall of the graft) that then propagates along the longitudinal axis of the tube.

Suture retention strength

Figure 9 shows a comparison of the SRS of electrospun tubes and relevant (porcine carotid and aortic arterial) vascular tissues. The 18 and 25 wt % tubes, in both the straight and oblique cut cases, failed at an average value of 3.7*N* similar to or greater than what has been observed elsewhere[11,20] and statistically identical to or greater than the natural tissues. Interestingly, the 12 wt % tubes had a much lower SRS—0.56*N*—while the 6.7 wt % PCL in HFIP samples were statistically identical to the 18 and 25 wt % cases. The HFIP samples, however, possessed a much broader range (almost 4*N* in the straight cut case) of values. The 12 wt % tubes displayed a much more narrow range of SRS values.

Of equal importance is that when the interface between synthetic and natural tissue was tested, failure always occurred in the arterial wall rather than in the graft. This demonstrated that the graft SRS is more than adequate. SEM [Fig. 10(a)] shows an image of the multifilament structures penetrating both sides of a graft–tissue interface. Figure 10(b) shows a representative image of an electrospun structure following suture pullout. The sutures appear to rip cleanly through the electrospun matrix.

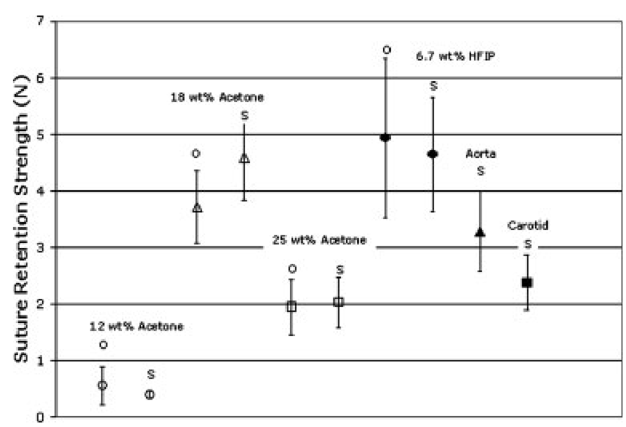

Figure 9. Suture retention strengths (S = straight cut; O = oblique cut) for the electrospun compositions versus natural tissues. With the exception of the electrospun 12 wt % PCL can meet or exceed this surgical requirement of matching natural tissues.

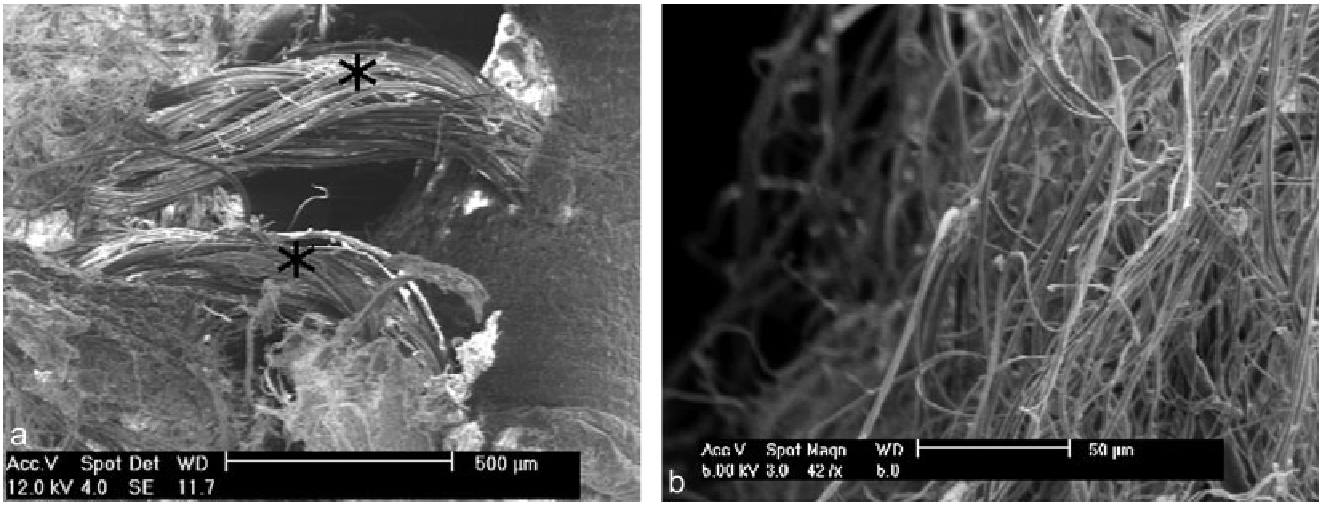

Figure 10. (a) Sutures (marked with an *) stabilizing an electrospun graft (left hand side of image)/tissue (right hand side of image) interface utilizing the procedure given previously. (b) Section of 18 wt% PCL through which the sutures in (a) have been pulled showing a clean failure.

DISCUSSION

The generation of scaffolds having tailored, biomimetic geometries (across multiple scales) has become an increasingly active area of research.[43,48,54–61] Electrospinning is an ideal method for achieving this in three-dimensional form, partly due to the ease with which it produces nonwoven nano- to micro-sized fibrous scaffolds having 70–90% relative porosity. Although electrospinning as a technique for vascular applications was first demonstrated in 1978,[35] many other fabrication techniques producing synthetic forms of tissue-engineered blood vessels have been studied: collagen gels,[19,62–64] polymer scaffolds[11,12,18,65–69], and self-assembly.[13,70] In spite of the successes of these alternative methods, electrospinning has enjoyed recent popularity due its inherent simplicity and affordability.

Electrospinning techniques have previously been used for synthetic graft fabrication. Xu et al. electrospun a block copolymer, poly(L-lactide-caprolactone (P[(LLA-CL)] (75:25)) and demonstrated that it had greater tensile strength and elongation than vascular tissue,[46] Boland et al. electrospun both collagen and elastin into tubes having appropriate physiological diameters,[71] Jeong et al. spun novel tubes consisting of a porous collagen matrix and an electrospun PLGA layer that substantially improved the mechanical strength of the collagen scaffold.[72] Stitzel et al. fabricated composite collagen, elastin, and poly(lactic-co-glycolic acid) (PLGA) scaffolds that displayed burst pressures of up to 1425 mmHg.[73] The majority of these investigations included some level of mechanical property characterization, but said little regarding the nature of the observed failures did not describe behavior at the microstructural level. We set out to more fully understand what factors, exactly, allow a mechanically capable graft to be electrospun. This relies heavily on previous work regarding point bonding concepts[51,54] potentially important in electrospun structures having a fortunate biomimetic resemblance to biologically produced ECM's.

Creating small diameter synthetic vascular grafts involves a number of challenges. The first challenge is to fabricate a structural matrix that possesses mechanical strength and flexibility sufficient to withstand high physiological pressures *in vivo* without being prone to aneurysm and graft dilation. Engineering-based approaches to such mechanical property goals often rely solely on tensile evaluations. In the context of vascular tissue engineering, however, burst pressure and SRS are more clinically relevant as they better describe a surgeon's immediate concerns regarding any new graft material. The former provides a measure of how likely these grafts can resist the blood pressures generated within the body. The prerequisite clinical benchmarks are well-described.[17,18,74] SRS, on the other hand, concerns a practical but equally important point: can these structures successfully retain the sutures used to hold the graft in place? We evaluate three parameters (tensile strength, burst pressure, and SRS) in the same context providing a direct, novel comparison of these different properties.

The microstructure of these engineered vascular graft prostheses also has an important role in modulating tissue ingrowth. Electrospun structures feature a morphological similarity to the extracellular matrix of natural tissues being characterized by a wide pore diameter distribution, high porosity and, as we show here, effective mechanical properties. The nanofibrous structures produced by the electrospinning process have a relatively (compared to standard Dacron) high surface area to volume ratio. Based on simple estimates of relative fiber diameter difference (~10 μm for Dacron;[75] ~1 μm for electrospun PCL) we estimate that the surface area of electrospun fiber is roughly 12 times greater thus making much more substrate available for cell attachment.

The mechanical properties of electrospun structures shown in Figures 1–3 reveal general trends in UTS, elongation, and modulus versus spinning conditions. The 12 wt % acetone material displays the lowest values in all three categories. Its tangential and longitudinal directions and the sheet condition are statistically indistinguishable. There appears to be little mechanical advantage in attempting to produce alignment from this particular solids loading. SEM (Fig. 4) shows that this condition contains point bonding that may compromise any potential mechanical property gains.

The 18 wt % longitudinal case shows the greatest elongation (up to 600%, Fig. 2), while its tangential direction and sheet condition are much lower and statistically indistinguishable. Strain in the longitudinal direction runs perpendicular to any existing alignment and generates a cellular arrangement of fibers[51], allowing maximum extension at minimal levels of applied force. Both the UTS and the moduli, however, are not statistically different between the three cases. This then suggests that point bonding[51,53] is significant enough to negate advantages gained by the alignment evident in the 18 wt % samples (Figs. 4 and 5).

The 25 wt % case shows no difference in either modulus, UTS, or elongation in the two directions. Interestingly, however, the sheet condition is both stronger and able to undergo greater elongation than either the tangential or the longitudinal directions. This suggests that the tubular deposition process can, in this circumstance, generate greater amounts of point bonding that compromise UTS and elongation.[51] Indeed, Figure 4 makes it clear that this composition is at the edge of "spinnability" and results in a strongly networked structure. Further increases in solids loading would likely lead to the generation of a largely solid polymer film interspersed with fiber-like features.

The use of HFIP introduces a solvent having greater volatility and higher dielectric strength, factors known to improve "spinnability."[76] This composition results in the classically expected effects of alignment (Fig. 5) on modulus (Fig. 3), UTS (Fig. 1), and elongation (Fig. 2) for both the tangential and longitudinal directions. The tangential direction has more than six times the strength of the longitudinal direction and more than three times that of the 18 wt % acetone case, the best performing acetone-based composition. The longitudinal direction shows both greater elongation and UTS as low as the 12 wt % acetone cases. What is more startling, however, is the behavior of the sheet condition comprised of completely unoriented fiber. Its modulus is identical to that of the highly aligned (Fig. 3) fiber. Elongation is only slightly higher than the tangential case, in spite of the absence of alignment. Although decreases in crystallinity versus increasing mandrel speed are well-established,[77,78] taken by itself this phenomenon would be expected to result in bulk property decreases; however, the opposite has been observed.[77,78] We suggest that individual electrospun fiber properties do not efficiently translate to the macroscale. In fact, the literature in this area reveals some ambiguity regarding the net efficiency of increased mandrel speed as a means of improving bulk properties. Net properties have been observed to either decrease[77] or remain unchanged in the tangential/circumferential and transverse/longitudinal directions.[79] Our observations of increased point bonding with increases in rotational speed provide evidence that point bonding can have more dominant effects on properties than alignment.

Figure 6 shows that we met or exceeded the goal set out at the beginning of this investigation. There appears to be an inherent thickness dependence, as increased deposition time provides greater burst pressure resistance. The desired thickness in any vascular application, however, varies greatly with physiological location and we plan to investigate this in more detail. The fact that burst pressure and tensile strength do not necessarily follow one another reflects the fact that the stress states are different. Tensile strain is applied uniaxially while bursting strain is biaxial, or applied in more than one direction at once. The latter more efficiently locates defects in the microstructure (Fig. 7) and leads to earlier failure. If these inherent defect populations could be quantified in terms of their size and ranked in descending order, we suspect that they would follow 18 wt % > 25 wt % > HFIP. This would largely explain the differences observed in Figure 6.

These observations prove that electrospun tubes can exhibit burst pressures that equal or surpass surgical standards. Figures 7 and 8 suggest that the mechanisms leading to failure in these structures involves (1) isolation of stress to areas of the scaffold having smaller diameters and thus greater compliance and thus easier expansion of pre-existing defects; (2) localized alignment of fiber in an arbitrary direction; and (3) fracture of these strained, highly aligned fibers leading to catastrophic failure in the longitudinal direction.

The SRS data clearly show that electrospun tubes can match or exceed the suture retention capabilities of relevant natural tissues. Only the 12 wt % acetone data are clearly weaker, an observation that fits the trend generated by the tensile, modulus, and burst pressure data. SEM (Fig. 10) shows that pull through of the suture occurs by relatively clean fracture of the matrix without significant permanent alignment or deformation of the surrounding fiber.

We are well aware that compliance matching is another factor critical to avoiding long-term occlusion. Compliance measurements[9] on these electrospun tubes are ongoing.

CONCLUSIONS

For any near term application of electrospun structures as vascular replacements, ensuring adequate mechanical properties is of paramount importance. By careful control of conditions, electrospun PCL tubes having burst pressures $>$ 2000 mmHg could be routinely synthesized. In the course of this study, we have injected biomimetic elements of vascular design by targeting fiber alignment to achieve improved mechanical properties. The expected positive effects of alignment can, however, be compromised by increased fiber-to-fiber point bonding. Electrospun structures displaying no discernable alignment could achieve clinically sufficient burst pressures. We link the microstructural characteristics of these burst pressure competent electrospun tubes to more standard mechanical properties. In the future, we will address another "missing link," the connection between compliance and microstructure.

Any opinions, findings, and conclusions or recommendations expressed in this material are those of the authors and do not necessarily reflect the views of the National Science Foundation. We also acknowledge the NSF Integrated Graduate Education and Research Training grant (Jim Lee, PI).

References

1. Lusis AJ. Atherosclerosis. Nature 2000;407:233–241.
2. Thom T, Haase N, Rosamond W, Howard VJ, Rumsfeld J, Manolio T, Zheng ZJ, Flegal K, O'Donnell C, Kittner S, Lloyd-Jones D, Goff DC, Hong YL, Adams R, Friday G, Furie K, Gorelick P, Kissela B, Marler J, Meigs J, Roger V, Sidney S, Sorlie P, Steinberger J, Wasserthiel-Smoller S, Wilson M, Wolf P. Heart disease and stroke statistics—2006 update—A report from the American Heart Association Statistics Committee and Stroke Statistics Subcommittee. Circulation 2006; 113:E85–E151.
3. Bos GW, Poot AA, Beugeling T, van Aken WG, Feijen J. Small-diameter vascular graft prostheses: Current status. Arch Physiol Biochem 1998;106:100–115.
4. Pevec WC, Darling RC, Litalien GJ, Abbott WM. Femoropopliteal reconstruction with knitted, nonvelour dacron versus expanded polytetrafluoroethylene. J Vasc Surg 1992;16:60–65.
5. Voorhees AJA, Ah B. The use of tube constructed from Vinyon "N" cloth in bridging arterial defects. Ann Surg 1952;135:332–336.
6. Heyligers JMM, Arts CHP, Verhagen HJM, de Groot PG, Moll FL. Improving small-diameter vascular grafts: From the application of an endothelial cell lining to the construction of a tissue-engineered blood vessel. Ann Vasc Surg 2005;19:448–456.
7. Anonymous. Collaborative overview of randomized trials of antiplatelet therapy. II. Maintenance of vascular graft or arterial patency by antiplatelet therapy. Br Med J 1994;308:159–168.
8. Herring MGA, Glover J. A single-stage technique for seeding vascular grafts with autogeneous endothelium. Surgery 1978;84:498–504.
9. Conklin BS, Richter ER, Kreutziger KL, Zhong DS, Chen C. Development and evaluation of a novel decellularized vascular xenograft. Med Eng Phys 2002;24:173–183.
10. Daniel J, Abe K, McFetridge PS. Development of the human umbilical vein scaffold for cardiovascular tissue engineering applications. ASAIO J 2005;51:252–261.
11. Hoerstrup SP, Zund G, Sodian R, Schnell AM, Grunenfelder J, Turina MI. Tissue engineering of small caliber vascular grafts. Eur J Cardiothorac Surg 2001;20:164–169.
12. Isaka M, Nishibe T, Okuda Y, Saito M, Seno T, Yamashita K, Izumisawa Y, Kotani T, Yasuda K. Experimental study on stability of a high-porosity expanded polytetrafluoroethylene graft in dogs. Ann Thorac Cardiovasc Surg 2006;12:37–41.
13. L'Heureux N, Dusserre N, Konig G, Victor B, Keire P, Wight TN, Chronos NAF, Kyles AE, Gregory CR, Hoyt G, Robbins RC, McAllister TN. Human tissue-engineered blood vessels for adult arterial revascularization. Nat Med 2006;12:361–365.
14. L'Heureux N, Paquet S, Labbe R, Germain L, Auger FA. A completely biological tissue-engineered human blood vessel. FASEB J 1998;12:47–56.
15. Mary C, Marois Y, King MW, Hong T, Laroche G, Douville Y, Martin L, Guidoin R. In vitro and in vivo studies of a polyester arterial prosthesis with a warp-knitted sharkskin structure. J Biomed Mater Res 1997;35:459–472.
16. McKee JA, Banik SSR, Boyer MJ, Hamad NM, Lawson JH, Niklason LE, Counter CM. Human arteries engineered in vitro. EMBO Rep 2003;4:633–638.
17. Niklason LE. Medical technology—Replacement arteries made to order. Science 1999;286:1493–1494.
18. Niklason LE, Gao J, Abbott WM, Hirschi KK, Houser S, Marini R, Langer R. Functional arteries grown in vitro. Science 1999;284:489–493.
19. Weinberg CB, Bell E. A blood-vessel model constructed from collagen and cultured vascular cells. Science 1986;231:397–400.
20. Xu J, Ge HY, Zhou XL, Yang DP, Guo TF, He J, Li Q, Hao ZH. Tissue-engineered vessel strengthens quickly under physiological deformation: Application of a new perfusion bioreactor with machine vision. J Vasc Res 2005;42:503–508.
21. Woodward SC, Brewer PS, Moatamed F. The intracellular degradation of poly(e-caprolactone). J Biomed Mater Res 1985;19:437–444.
22. Fujihara K, Kotaki M, Ramakrishna S. Guided bone regeneration membrane made of polycaprolactone/calcium carbonate composite nano-fibers. Biomaterials 2005;26:4139–4147.
23. Shin M, Yoshimoto H, Vacanti Joseph P. In vivo bone tissue engineering using mesenchymal stem cells on a novel electrospun nanofibrous scaffold. Tissue Eng 2004;10:33–41.
24. Yoshimoto H, Shin YM, Terai H, Vacanti JP. A biodegradable nanofiber scaffold by electrospinning and its potential for bone tissue engineering. Biomaterials 2003;24:2077–2082.
25. Wutticharoenmongkol P, Sanchavanakit N, Pavasant P, Supaphol P. Novel bone scaffolds of electrospun polycaprolactone

fibers filled with nanoparticles. J Nanosci Nanotechnol 2006;6:514–522.
26. Li W-J, Danielson KG, Alexander PG, Tuan RS. Biological response of chondrocytes cultured in three-dimensional nanofibrous poly(e-caprolactone) scaffolds. J Biomed Mater Res Part A 2003;67A:1105–1114.
27. Li W-J, Tuli R, Huang X, Laquerriere P, Tuan RS. Multilineage differentiation of human mesenchymal stem cells in a three-dimensional nanofibrous scaffold. Biomaterials 2005;26:5158–5166.
28. Li WJW-J, Tuli R, Okafor C, Derfoul A, Danielson KGKG, Hall DJDJ, Tuan RSRS. A three-dimensional nanofibrous scaffold for cartilage tissue engineering using human mesenchymal stem cells. Biomaterials 2005;26:599–609.
29. Nam J, Huang Y, Agarwal S, Lannutti J. Materials selection and residual solvent retention in biodegradable electrospun fibers. J Appl Polym Sci 2007;107:1547–1554.
30. Nam J, Huang Y, Agarwal S, Lannutti J. Improved cellular infiltration in electrospun fiber via engineered porosity. Tissue Eng 2007;13:2249–2257.
31. Lannutti J, Reneker D, Ma T, Tomasko D, Farson D. Electrospinning for tissue engineering scaffolds. Mater Sci Eng C 2007;27:504–509.
32. Choi HW, Johnson JK, Nam J, Farson DF, Lannutti JJ. Structuring electrospun polycaprolactone nanofiber tissue scaffolds by femtosecond laser ablation. J Laser Appl 2007;19:125–134.
33. Ayodeji O, Graham E, Kniss D, Lannutti J, Tomasko D. Carbon dioxide impregnation of electrospun polycaprolactone fibers. J Supercrit Fluids 2007;41:173–178.
34. Wnek GE, Carr ME, Simpson DG, Bowlin GL. Electrospinning of nanofiber fibrinogen structures. Nano Lett 2003;3:213–216.
35. Annis D, Bornat A, Edwards RC, Highamm A, Loveday B, Wilson J. An elastomeric vascular prosthesis. Trans Am Soc Artif Intern Organs 1978;29:209–214.
36. Berry JP. US Pat. 4965110 (1990).
37. Bornat A. Production of electrostatically spun products. US Pat.4689186 (1987).
38. Lee KH, Kim HY, Khil MS, Ra YM, Lee DR. Characterization of nano-structured poly(epsilon-caprolactone) nonwoven mats via electrospinning. Polymer 2003;44:1287–1294.
39. Zong XH, Kim K, Fang DF, Ran SF, Hsiao BS, Chu B. Structure and process relationship of electrospun bioabsorbable nanofiber membranes. Polymer 2002;43:4403–4412.
40. Venugopal J, Ramakrishna S. Applications of polymer nanofibers in biomedicine and biotechnology. Appl Biochem Biotechnol 2005;125:147–157.
41. Pawlowski KJ, Rittgers SE, Schmidt SP, Bowlin GL. Endothelial cell seeding of polymeric vascular grafts. Front Biosci 2004;9:1412–1421.
42. Courtney T, Sacks MS, Stankus J, Guan J, Wagner WR. Design and analysis of tissue engineering scaffolds that mimic soft tissue mechanical anisotropy. Biomaterials 2006;27:3631–3638.
43. Katta P, Alessandro M, Ramsier RD, Chase GG. Continuous electrospinning of aligned polymer nanofibers onto a wire drum collector. Nano Lett 2004;4:2215–2218.
44. Li D, Wang YL, Xia YN. Electrospinning nanofibers as uniaxially aligned arrays and layer-by-layer stacked films. Adv Mater 2004;16:361–366.
45. Teo WE, Kotaki M, Mo XM, Ramakrishna S. Porous tubular structures with controlled fibre orientation using a modified electrospinning method. Nanotechnology 2005;16:918–924.
46. Xu CY, Inai R, Kotaki M, Ramakrishna S. Aligned biodegradable nanotibrous structure: A potential scaffold for blood vessel engineering. Biomaterials 2004;25:877–886.
47. Yang F, Murugan R, Wang S, Ramakrishna S. Electrospinning of nano/micro scale poly(L-lactic acid) aligned fibers and their potential in neural tissue engineering. Biomaterials 2005;26:2603–2610.
48. Zhang Y, Ouyang H, Lim Chwee T, Ramakrishna S, Huang Z-M. Electrospinning of gelatin fibers and gelatin/PCL composite fibrous scaffolds. J Biomed Mater Res B Appl Biomater 2005;72:156–165.
49. Gaumer J, Lannutti J. Source-to-ground distance and the mechanical properties of electrospun fiber. J Appl Polym Sci 2008, submitted.
50. ANSI/AAMI/ISO.8.3.3.3 Determination of pressurized burst strength—Cardiovascular implants-tubular vascular prostheses. 7198: 2004.
51. Johnson J, Ghosh A, Lannutti J. Microstructure-property relationships in a tissue engineering scaffold. J Appl Polym Sci 2007;104:2919–2927.
52. ANSI/AAMI/ISO.8.8 Determination of suture retention strength cardiovascular implants-tubular vascular prostheses. 7198: 2004.
53. Inai R, Kotaki M, Ramakrishna S. Deformation behavior of electrospun poly(L-lactide-co-epsilon-caprolactone) nonwoven membranes under uniaxial tensile loading. J Polym Sci B Polym Phys 2005;43:3205–3212.
54. Huang ZM, Zhang YZ, Ramakrishna S. Double-layered composite nanofibers and their mechanical performance. J Poly Sci B Polym Phys 2005;43:2852–2861.
55. Boland ED, Wnek GE, Simpson DG, Pawlowski KJ, Bowlin GL. Tailoring tissue engineering scaffolds using electrostatic processing techniques: A study of poly(glycolic acid) electrospinning. J Macromol Sci Pure Appl Chem 2001;38:1231–1243.
56. Gong HJ, Yang XP, Chen GQ, Liu TQ, Zhang SM, Deng XL, Hu XY. Study on PLA/MWNT/HA hybrid nanofibers prepared via electrospinning technology. Acta Polymerica Sinica 2005;2:297–300.
57. Ito Y, Hasuda H, Kamitakahara H, Ohtsuki C, Tanihara M, Kang IK, Kwon OH. A composite of hydroxyapatite with electrospun biodegradable nanofibers as a tissue engineering material. J Biosci Bioeng 2005;100:43–49.
58. Ma ZW, Kotaki M, Inai R, Ramakrishna S. Potential of nanofiber matrix as tissue-engineering scaffolds. Tissue Eng 2005;11:101–109.
59. Reneker DH, Haoqing H. Electrospinning. In: Wnek GE, Bowlin G, editors. Encyclopedia of Biomaterials and Biomedical Engineering; Taylor & Francis Group, LLC 2004. p 543–550.
60. Riboldi SA, Sampaolesi M, Neuenschwander P, Cossu G, Mantero S. Electrospun degradable polyesterurethane membranes: Potential scaffolds for skeletal muscle tissue engineering. Biomaterials 2005;26:4606–4615.
61. Kalayci VE, Patra PK, Buer A, Ugbolue SC, Kim YK, Warner SB. Fundamental investigations on electrospun fibers. J Adv Mater 2004;36:43–47.
62. Seliktar D, Black RA, Vito RP, Nerem RM. Dynamic mechanical conditioning of collagen-gel blood vessel constructs induces remodeling in vitro. Ann Biomed Eng 2000;28:351–362.
63. Ziegler T, Alexander RW, Nerem RM. An endothelial cell-smooth muscle-cell coculture model for use in the investigation of flow effects on vascular biology. Ann Biomed Eng 1995;23:216–225.
64. Girton TS, Oegema TR, Grassl ED, Isenberg BC, Tranquillo RT. Mechanisms of stiffening and strengthening in media-equivalents fabricated using glycation. J Biomech Eng Trans ASME 2000;122:216–223.
65. Schmidt CE, Baier JM. Acellular vascular tissues: Natural biomaterials for tissue repair and tissue engineering. Biomaterials 2000;21:2215–2231.
66. Niklason LE, Langer RS. Advances in tissue engineering of blood vessels and other tissues. Transpl Immunol 1997;5:303–306.

67. Ishii Y, Kronengold RT, Virmani R, Rivera EA, Goldman SM, Prechtel EJ, Schuessler RB, Damiano RJ. Novel bioengineered small caliber vascular graft with excellent one-month patency. Ann Thorac Surg 2007;83:517–525.
68. Veith FJ, Gupta SK, Ascer E, Whiteflores S, Samson RH, Scher LA, Towne JB, Bernhard VM, Bonier P, Flinn WR, Astelford P, Yao JST, Bergan JJ. 6-Year prospective multicenter randomized comparison of autologous saphenous-vein and expanded polytetrafluoroethylene grafts in infrainguinal arterial reconstructions. J Vasc Surg 1986;3:104–114.
69. Chard RB, Johnson DC, Nunn GR, Cartmill TB. Aorta-coronary bypass-grafting with polytetrafluoroethylene conduits—Early and late outcome in 8 patients. J Thorac Cardiovasc Surg 1987;94:132–134.
70. L'Heureux N, Paquet S, Labbe R, Germain L, Auger FA. A completely biological tissue-engineered human blood vessel. FASEB J 1998;12:47–56.
71. Boland ED, Matthews JA, Pawlowski KJ, Simpson DG, Wnek GE, Bowlin GL. Electrospinning collagen and elastin: Preliminary vascular tissue engineering. Front Biosci 2004;9:1422–1432.
72. Jeong SI, Kim SY, Cho SK, Chong MS, Kim KS, Kim H, Lee SB, Lee YM. Tissue-engineered vascular grafts composed of marine collagen and PLGA fibers using pulsatile perfusion bioreactors. Biomaterials 2007;28:1115–1122.
73. Stitzel J, Liu L, Lee SJ, Komura M, Berry J, Soker S, Lim G, Van Dyke M, Czerw R, Yoo JJ, Atala A. Controlled fabrication of a biological vascular substitute. Biomaterials 2006;27:1088–1094.
74. Niklason LE, Abbott W, Gao JM, Klagges B, Hirschi KK, Ulubayram K, Conroy N, Jones R. Morphologic and mechanical characteristics of engineered bovine arteries. J Vasc Surg 2001;33:628–638.
75. Recum AFV. Handbook of Biomaterials Evaluation. Macmillan, New York, NY; 1986.
76. Ramakrishna S, Fujihara K, Teo W-E, Lim T-C, Ma Z. An Introduction to Electrospinning and Nanofibers. World Scientific, New Jersey; 2005. 396 p.
77. Kim KW, Lee KH, Khil MS, Ho YS, Kim HY. Fibers and Polymers. The effect of molecular weight and the linear velocity of drum surface on the properties of electrospun poly(ethylene terephthalate) nonwovens. 2004;5:122–127.
78. Thomas V, Jose MV, Chowdhury S, Sullivan JF, Dean DR, Vohra YK. Mechano-morphological studies of aligned nanofibrous scaffolds of polycaprolactone fabricated by electrospinning. J Biomater Sci Polym Ed 2006;17:969–984.
79. Matsuda T, Ihara M, Inoguchi H, Kwon K, Takamizawa K, Kidoaki S. Mechano-active scaffold design of small-diameter artificial graft made of electrospun segmented polyurethane fabrics. J Biomed Mater Res Part A 2005;73A:125–131.